# Inclined magnetic structure of iron borate $Pr_xY_{1-x}Fe_3(BO_3)_4$: A neutron diffraction study and crystal-field calculations

C. Ritter,[1] A. I. Pankrats,[2,3] A. A. Demidov,[4] D. A. Velikanov,[2] V. L. Temerov,[2] and I. A. Gudim[2]

[1]*Institute Laue-Langevin, BP 156, F-38042 Grenoble, France*

[2]*L. V. Kirensky Institute of Physics, Siberian Branch of RAS, 660036 Krasnoyarsk, Russia*

[3]*Siberian Federal University, 660041 Krasnoyarsk, Russia*

[4]*Bryansk State Technical University, 241035 Bryansk, Russia*

(Received 18 February 2015; revised manuscript received 23 March 2015; published 13 April 2015)

The magnetic structure of the mixed rare-earth system $Pr_xY_{1-x}Fe_3(BO_3)_4$ has been studied by elastic neutron powder diffraction and magnetic measurements. A spin reorientation from easy axis to easy plane occurs in the concentration range $x = 0.67$–$0.45$ through the formation of inclined magnetic structures. The inclination of the Fe moments from the basal plane depends on the Pr content and ranges from 67(2)° for $x = 0.67$ to 16(4)° for $x = 0.45$ at $T = 3$ K. A nonmonotonic change of the inclination angle with temperature is found for all compounds but there is no sign of a spontaneous spin reorientation in the temperature range of magnetic order.

An approach based on a crystal-field model for the $Pr^{3+}$ ion and on the molecular-field approximation is used to describe the magnetic characteristics of the system $Pr_xY_{1-x}Fe_3(BO_3)_4$. A good agreement between the experimental and calculated temperature dependences of the magnetic susceptibilities and the angle of inclination of Fe moments from the basal plane has been achieved.

DOI: 10.1103/PhysRevB.91.134416 PACS number(s): 75.30.−m, 75.40.Cx, 75.50.Ee, 71.70.−d

## I. INTRODUCTION

$Pr_xY_{1-x}Fe_3(BO_3)_4$ belongs to the family of rare-earth ferroborates $RFe_3(BO_3)_4$ that exhibit a variety of phase transitions and some multiferroic features (see, e.g., Refs. [1–5]). Crystallizing in the noncentrosymmetric trigonal space group $R32$ a structural transition to $P3_121$ can take place on cooling at a temperature depending linearly on the rare-earth ionic radius [6,7]. While in $ErFe_3(BO_3)_4$ with $r(Er^{3+}) = 0.89$ Å this transition is found above 520 K [8], $EuFe_3(BO_3)_4$ with $r(Eu^{3+}) = 0.947$ Å sees it at about 80 K [6]. $SmFe_3(BO_3)_4$ ($r(Sm^{3+}) = 0.96$ Å) seems to be on the borderline of keeping the $R32$ structure even at the lowest temperatures [9] like all the other $RFe_3(BO_3)_4$ compounds containing an even lighter rare earth.

The Fe subsystem in pure $YFe_3(BO_3)_4$ is ferromagnetically ordered in the basal $ab$ plane with magnetic moments lying in the plane and adjacent planes in direction of the rhombohedral $c$ direction being antiferromagnetically aligned [10–12]. Despite the presence of well separated helicoidal Fe chains extending along the rhombohedral $c$ axis, the interchain exchange interaction Fe-O-B-O-Fe through a $BO_3$ group is of the same order of magnitude as the intrachain Fe-O-Fe interaction, and there are no signs of a low dimensional magnetic behavior. This view was confirmed by density functional theory (DFT) calculations made for $TbFe_3(BO_3)_4$ in Ref. [13]. A similar result is given in phenomenological calculations (see, e.g., Refs. [3] and [14–16]) where the magnetic properties of several $RFe_3(BO_3)_4$ compounds are described using a crystal-field model for the $R$ ion and a molecular field approximation.

The common property of all the $RFe_3(BO_3)_4$ compounds is the weak exchange interaction of the $R$ subsystem; no long range magnetism is established on the $R$ sublattice if Fe is replaced by nonmagnetic Al [17]. However, the magnetic order still occurs simultaneously in both subsystems at the Néel temperature of the Fe subsystem due to the exchange interaction between $R^{3+}$ and $Fe^{3+}$ ions [18,19]. There are no exchange interactions of type Fe–O–$R$ within one basal $ab$ layer, each $R^{3+}$ ion is coupled by exchange interactions only with $Fe^{3+}$ ions from the adjacent basal layers belonging to the same antiferromagnetic sublattice. Taking into account a ferromagnetic exchange interaction between the iron $3d$ spin and the spin part of the total moment $J$ of the rare earth, the parallel alignment of magnetic moments of $Fe^{3+}$ and $R^{3+}$ ions occurs within the basal layers due to the spin-orbit coupling for light rare earths with $J = |L - S|$ and the antiparallel alignment of magnetic moments—for heavy rare earths with $J = L + S$ [9,20].

Due to the polarizing effect of the iron subsystem on the rare-earth one, the magnetic anisotropy of $RFe_3(BO_3)_4$ compounds is determined by the contributions of both subsystems. Depending on the magnitude and the sign of the anisotropic contribution of the rare-earth subsystem, easy-axis (EA) or easy-plane (EP) magnetic structures can be established in the crystal. As detailed neutron scattering results show, these structures can be slightly noncollinear ($R$ = Ho [11] and Er [8]) or long period incommensurate ($R$ = Nd [21] and Gd above 10 K [22]).

In crystals with $R$ = Gd and Ho, the competing magnetic anisotropy contributions of $R$ and Fe subsystems have opposite signs but are of similar magnitude. The difference in the temperature dependences of the contributions leads, in these crystals, to spontaneous transitions between low temperature EA and high temperature EP states at $T_{SR} = 10$ K for Gd [12,23] and 4.7 K for Ho [11,24].

The magnetic anisotropy of mixed rare-earth compounds with $R = Nd_xDy_{1-x}$ has been shown to be determined as well by the competition of EP contributions from the $Nd^{3+}$ and $Fe^{3+}$ ions on the one hand and the EA contribution from the $Dy^{3+}$ ions on the other hand. As a result, spontaneous reorientation transitions between EP and EA states occur also in these complex crystals with the temperature $T_{SR}$ depending on $x$ [25,26].

 

The relation between the competing contributions can be changed by a diamagnetic dilution of one of the subsystems reducing the contribution of the subsystem to the crystal anisotropy. Thus, in a crystal with $R = \mathrm{Gd}$, the diamagnetic dilution of the iron subsystem with $Ga^{3+}$ ions reduces the anisotropic contribution of the $Fe^{3+}$ subsystem. As a result, the contribution of the gadolinium subsystem appears to be prevalent and, in the absence of a magnetic field, the crystal $GdFe_{3-x}Ga_x(BO_3)_4$ remains an EA antiferromagnet in the entire range of magnetic ordering [27].

In $PrFe_3(BO_3)_4$, the contribution of the $Pr^{3+}$ ions to the magnetic anisotropy of the crystal is dominant and defines an EA antiferromagnetic structure at all temperatures below the Néel temperature $T_N = 32\,\mathrm{K}$ [8,28]. We can expect that a diamagnetic dilution of the subsystem of $Pr^{3+}$ ions by nonmagnetic ions $Y^{3+}$ ions weakens the EA contribution of praseodymium and, at a certain yttrium concentration, will lead to a transition to the EP magnetic structure.

To study this possibility, we have grown a family of crystals $Pr_xY_{1-x}Fe_3(BO_3)_4$ and investigated their magnetic properties. Magnetic measurements, details of which will be published elsewhere, show that the critical concentration is near to $x = 0.55$. Neutron scattering data found that the transition from the EA to the EP structure occurs in this family through the formation of inclined magnetic structures in the concentration range $x = 0.67$–$0.45$. The inclination of the Fe moment from the principal axis increases with Y content.

## II. EXPERIMENT DETAILS

### A. Sample preparation

Samples were prepared at the Institute of Physics in Krasnoyarsk. Single crystals have been grown from fluxes based on trimolybdate bismuth $(100–n)\,\mathrm{mass\%}\{Bi_2Mo_3O_{12} + 3^{11}B_2O_3 + 0.5[xPr_2O_3 + (1–x)Y_2O_3]\} + n\,\mathrm{mass\%}\,Pr_xY_{1-x}Fe_3(^{11}BO_3)_4$ [29]. For the concentration $n = 20$, the saturation temperature $T_s$ was $T_s \approx 950\,^\circ\mathrm{C}$, and its concentration dependence can be described as $dT_s/dn \approx 6\,^\circ\mathrm{C/mass\%}$. Fluxes with a mass of 100 g were prepared. Crystals were grown upon seeds at a starting temperature $T = T_s–7\,^\circ\mathrm{C}$ reducing the temperature by $1\,^\circ\mathrm{C/day}$ over 5 days. Single crystals of about 4–6 mm in size were grown. The neutron diffraction measurements were performed on powders of grown crystals with $x = 0.67$, 0.55, and 0.45.

### B. Neutron diffraction and magnetization measurements

Neutron diffraction data were taken at the Institute Laue-Langevin in Grenoble, France, using the high resolution powder diffractometer D2B ($\lambda = 1.594\,\text{Å}$) and the high flux powder diffractometers D1B ($\lambda = 2.52\,\text{Å}$) and D20 ($\lambda = 2.41\,\text{Å}$). The temperature dependencies of the neutron diffraction patterns (thermodiffractogram) were measured for $x = 0.67$ on D1B taking a spectrum every 30 min between 3 and 35 K, with a temperature resolution of 1.1 K and for $x = 0.55$ on D20 taking a spectrum every 6 min between 1.8 and 38 K with $\Delta T = 0.7\,\mathrm{K}$. All three compounds were further measured on D2B between base temperature and about 40 K taking spectra every 2 K and at room temperature. All data were refined by the Rietveld method using the FullProf [30] program. Magnetic symmetry analysis was done using the program BASIREPS, which is included in the FullProf suite [31,32]. Magnetic measurements were performed at the Institute of Physics in Krasnoyarsk using the Magnetic Properties Measurement System (MPMS)-5 (Quantum Design). The temperature interval was 2–300 K in magnetic fields up to 5 T.

## III. RESULTS AND DISCUSSION

The crystallographic details of the three compounds were determined using the high resolution data taken at room temperature on D2B with $\lambda = 1.594\,\text{Å}$. Details of the refined results are presented in Table I; Fig. 1 displays an example of the refinement of $Pr_{0.45}Y_{0.55}Fe_3(BO_3)_4$. At room temperature, all three compounds crystallize in the space group $R32$ as expected from the calculated average $R^{3+}$ size. Assuming the abovementioned linear trend for the transition temperature as a function of the $R^{3+}$ ionic radius [6], the $x = 0.67$ compound should not undergo a transition to $P3_121$ on lowering the temperature, while a transition should appear for the $x = 0.55$ and 0.45 compounds at temperatures of about 65 and 140 K, respectively. All compounds are free from impurities.

TABLE I. Lattice constants, atomic coordinates, interatomic distances at 300 K for $Pr_xY_{1-x}Fe_3(BO_3)_4$ in $R32$ or $P3_121$ ($x = 0$). Results for $x = 1$ are taken from Ref. [8] and for $x = 0$ from Ref. [11]. For $x = 0$, the interatomic distances given are average values.

| | $x = 1$ | $x = 0.67$ | $x = 0.55$ | $x = 0.45$ | $x = 0$ |
|---|---|---|---|---|---|
| $a$ (Å) | 9.5927(1) | 9.5636(1) | 9.5622(1) | 9.5601(1) | 9.5251(1) |
| $c$ (Å) | 7.6208(1) | 7.5912(1) | 7.5883(1) | 7.5855(1) | 7.5558(1) |
| Vol. (Å$^3$) | 607.3 | 601.3 | 600.9 | 600.4 | 593.7 |
| Fe (*9d*) $x$ | 0.5510(2) | 0.5503(1) | 0.5499(1) | 0.5499(1) | |
| O1 (*9e*) $x$ | 0.8546(4) | 0.8552(3) | 0.8550(3) | 0.8552(3) | |
| O2 (*9e*) $x$ | 0.5896(3) | 0.5914(3) | 0.5906(3) | 0.5920(2) | |
| O3 (*18f*) $x$ | 0.0266(2) | 0.0267(2) | 0.0256(2) | 0.0261(1) | |
| $y$ | 0.2152(2) | 0.2141(2) | 0.2131(2) | 0.2129(2) | |
| $z$ | 0.1861(2) | 0.1835(3) | 0.1832(3) | 0.1827(2) | |
| B2 (*9e*) $x$ | 0.4455(2) | 0.4462(2) | 0.4467(2) | 0.4471(2) | |
| $R$-O3 (Å) | 2.410(2) | 2.382(2) | 2.376(2) | 2.370(2) | 2.343(8) |
| Fe-Fe (Å) | 3.186(1) | 3.181(1) | 3.184(1) | 3.183(1) | 3.175(4) |
| $R_{\mathrm{Bragg}}$ | 4.9 | 3.8 | 5.5 | 4.4 | 3.5 |

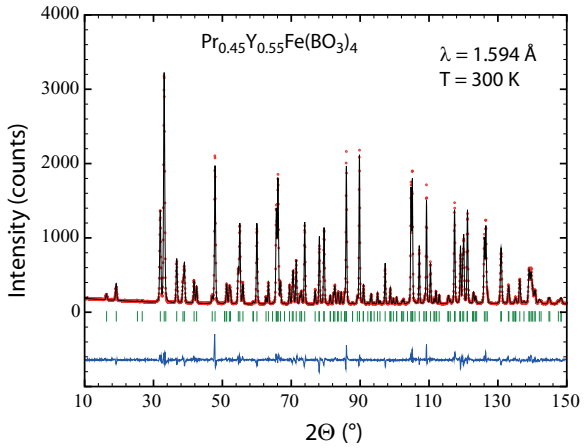


FIG. 1. (Color online) Observed (red dots), calculated (black line), and difference pattern of $Pr_{0.45}Y_{0.55}Fe_3(BO_3)_4$ at 300 K refined in $R32$. The tick marks indicate the calculated position of the Bragg peaks.

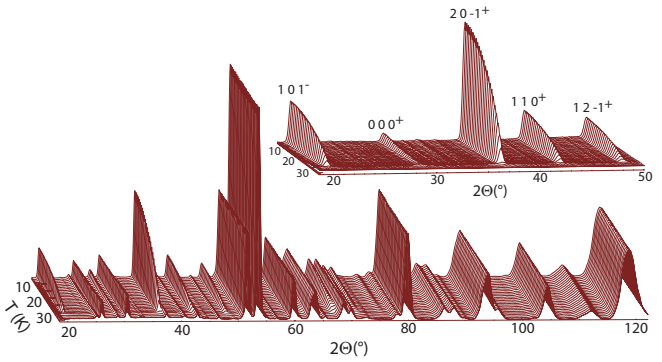


FIG. 2. (Color online) Thermal dependence of the neutron diffraction pattern of $Pr_{0.67}Y_{0.33}Fe(BO_3)_4$ ($\lambda = 2.52$ Å). The inset displays the low angle region of a difference thermodiffractogram created by subtracting the paramagnetic data set taken at 34 K, leaving only the magnetic scattering. The magnetic Bragg peaks are indexed using the magnetic propagation vector $\boldsymbol{\kappa} = [0\,0\,3/2]$.

Table I shows that the volume decreases by about 1% when going from the undoped $x = 1$ compound to the strongly doped $x = 0.45$ compound. Keeping the atomic coordinates fixed this should lead to a decrease of the $R$-O3 and Fe-Fe distances of about 0.4%. This has to be compared to the actual values resulting from the combined effect of the volume contraction and the shift of atomic positions which show that the $R$-O3 distance reduces by 1.7%, while the Fe-Fe distance stays nearly constant when going from $x = 1$ to $x = 0.45$. This underlines the backbone character of the helicoidal Fe chains within the $R\mathrm{Fe_3(BO_3)_4}$ compounds.

Figure 2 shows the thermal dependence of the high intensity neutron diffraction patterns (thermodiffractogram) of $Pr_{0.67}Y_{0.33}Fe_3(BO_3)_4$ between 3 and 34 K. Additional reflections can be seen to appear at around 30 K. These reflections are of magnetic origin and can be indexed with the magnetic propagation vector $\boldsymbol{\kappa} = [0\,0\,3/2]$. The magnetic peaks appearing are apart from the $(000^+)$ reflection, very similar to those already found for the pure compound $PrFe_3(BO_3)_4$, which sees a collinear alignment of Fe and Pr moments along the $c$ direction [8].

Magnetic symmetry analysis using the program BASIREPS was performed to determine the allowed irreducible

TABLE II. IR and their BV for $\boldsymbol{\kappa} = [0\,0\,2/3]$ in $R32$, $a = 0.5$, and $b = 0.866$.

| Fe on $x$ 0 0 | BV1 | BV2 | BV3 | BV4 | BV5 | BV6 |
|---|---|---|---|---|---|---|
| IR1: $x, y, z$ | 1 0 0 | | | | | |
| | 0 0 0 | | | | | |
| $-y, x-y, z$ | 0 1 0 | | | | | |
| | 0 0 0 | | | | | |
| $-x+y, -x, z$ | −1 −1 0 | | | | | |
| | 0 0 0 | | | | | |
| IR2: $x, y, z$ | 1 2 0 | 0 0 1 | | | | |
| | 0 0 0 | 0 0 0 | | | | |
| $-y, x-y, z$ | −2 −1 0 | 0 0 1 | | | | |
| | 0 0 0 | 0 0 0 | | | | |
| $-x+y, -x, z$ | 1 −1 0 | 0 0 1 | | | | |
| | 0 0 0 | 0 0 0 | | | | |
| IR3: $x, y, z$ | 1 0 0 | 0 1 0 | 0 0 1 | −a 0 0 | a a 0 | 0 0 a |
| | 0 0 0 | 0 0 0 | 0 0 0 | −b 0 0 | b b 0 | 0 0 b |
| $-y, x-y, z$ | 0 −a 0 | a a 0 | 0 0 −a | 0 1 0 | 1 0 0 | 0 0 −1 |
| | 0 −b 0 | b b 0 | 0 0 −b | 0 0 0 | 0 0 0 | 0 0 0 |
| $-x+y, -x, z$ | a a 0 | −a 0 0 | 0 0 −a | a a 0 | 0 −a 0 | 0 0 a |
| | −b −b 0 | b 0 0 | 0 0 b | −b b 0 | 0 b 0 | 0 0 −b |
| Pr on 0 0 0 | | | | | | |
| IR2: $x, y, z$ | 0 0 1 | | | | | |
| | 0 0 0 | | | | | |
| IR3: $x, y, z$ | 3a 0 0 | 0 3a 0 | | | | |
| | −b −2b 0 | −2b −b 0 | | | | |

representations (IR) and their basis vectors (BV); these are listed in Table II. For $PrFe_3(BO_3)_4$ it had been shown in Ref. [8] that the magnetic structure follows IR2. Neither IR2 nor IR1 can, however, create magnetic intensity for the $(000^+)$ reflection, which is absent for $x = 1.0$ but clearly present for $x = 0.67$. Testing IR3, it became quickly clear that this IR is also not able to reproduce the measured magnetic intensities.

Remembering that the magnetic structure of the $x = 0$ compound $YFe_3(BO_3)_4$ consists of a collinear alignment of the Fe moments within the basal $ab$ plane, a refinement of high resolution data taken at $T = 1.5$ K was done for $Pr_{0.67}Y_{0.33}Fe_3(BO_3)_4$, where a spin canting of the moments towards the basal plane was allowed resulting in an inclined spin structure state. This refinement converged immediately and resulted in magnetic moment values of $\mu^{Fe} = 4.2(1)\,\mu_B$ and $\mu^{Pr} = 0.8(3)\,\mu_B$. Figure 3(a) displays the magnetic structure where the size of the Pr moment has been exaggerated; Fig. 3(b) shows a plot of the refined data. Note that the $R$ sites in Fig. 3(a) are statistically occupied by $x Pr^{3+}$ and $(1–x)Y^{3+}$ ions and that the given magnetic moment value $\mu^{Pr}$ corresponds to the magnetic moment per actual $Pr^{3+}$ ion present. Within the hexagonal layers, the magnetic moments of the rare-earth sublattice are oriented parallel to the Fe sublattice as far as their $z$ components are concerned ($\mu_z^{Pr} = 0.7(2)\,\mu_B$), while the basal plane component is oriented antiparallel ($\mu_x^{Pr} = 0.4(3)\,\mu_B$). The behavior of the $z$ components is identical to the situation in the pure $PrFe_3(BO_3)_4$, while the antiparallel alignment of $R$ sublattice and Fe sublattice within the basal plane is the same as in $HoFe_3(BO_3)_4$ for $T > 4.7$ K [11].

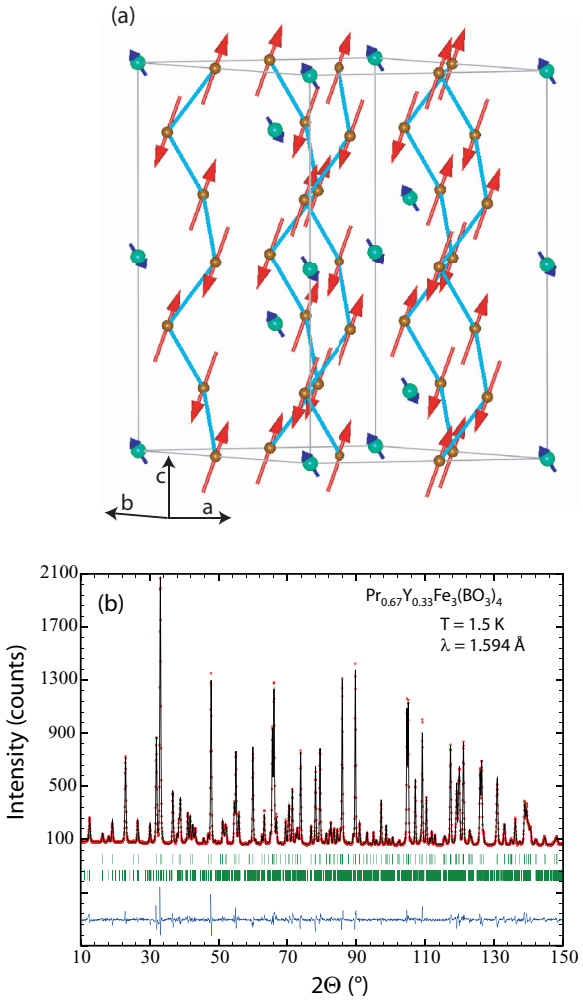


FIG. 3. (Color online) (a) Magnetic structure of $Pr_{0.67}Y_{0.33}Fe_3(BO_3)_4$. Pr moments in blue, Fe spins in red, and the direct Fe-Fe exchange along the helicoidal chains is indicated by light blue lines. (b) Observed (red dots), calculated (black line), and difference pattern of $Pr_{0.67}Y_{0.33}Fe_3(BO_3)_4$ at 1.5 K refined in $R32$. The tick marks indicate the calculated position of the nuclear (upper row) and magnetic (lower) Bragg peaks.

Misalignments of Fe and $R$ moments were found earlier by neutron research in other $RFe_3(BO_3)_4$ compounds. In $SmFe_3(BO_3)_4$, which adopts the EP structure, the magnetic moments of iron and samarium are predominantly aligned parallel having, however, a canting angle of about 70° relative to each other within the basal plane [9]. $ErFe_3(BO_3)_4$ having as well EP anisotropy sees a predominantly antiparallel order of Fe and Er moments within the basal plane with Fe moments slightly canted from the basal plane by an angle of ∼14° [8]. A similar magnetic structure is found in $HoFe_3(BO_3)_4$ above $T_{SR} = 4.7$ K [11]. Below this temperature, the EA structure appears with Fe moments ordered along the main axis and Ho moments slightly canted from the axis. In $Pr_xY_{1-x}Fe_3(BO_3)_4$, we have a situation in which the alignment (parallel or antiparallel) of the $R$ and Fe sublattices is not the same along the $c$ axis and within the basal plane. This result cannot be explained within the framework of a single isotropic exchange interaction. Instead, such a mutual orientation of the moments of praseodymium and iron requires opposite signs of the exchange interactions of the spin components oriented along the main axis and perpendicular to it. The physical reasons behind this anisotropy of the exchange interactions remain, however, unclear for the moment.

$HoFe_3(BO_3)_4$ is the only compound up to now where a spontaneous spin reorientation as a function of temperature has been followed directly by neutron diffraction [11]. Below 4.7 K, the magnetic moments that are lying in the basal plane change abruptly into the direction of the $c$ axis. In order to verify whether any spin reorientation takes place in $Pr_{0.67}Y_{0.33}Fe_3(BO_3)_4$, the temperature dependence of the magnetic moments was refined using the high intensity D1B data [33]. Figure 4(a) shows the thermal evolution of the total Fe and Pr moments, while Fig. 4(b) shows those of the basal plane component ($\mu_x^{Fe}$) and of the component in $z$ direction ($\mu_z^{Fe}$) of the Fe moment. Both sublattice magnetizations appear at the same temperature $T_N \approx 31$ K, and their evolution seems to be steady. Only when inspecting the individual components of the Fe moment [Fig. 4(b)] can a slight change in the temperature evolution of its basal plane component be discerned at about 10 K. Figure 4(c) shows how this leads to a small change of about 2° in the inclination $\Theta^{Fe}$ of the Fe moment between 10 and 3 K. This small change at low temperatures has to be compared to the reorientation of 90° of the Fe sublattice as found in the Ho compound.

Discussing the appearance of long range magnetic order in the series of $RFe_3(BO_3)_4$ compounds, it has been said [8,9,11,21,22] that the rare-earth sublattice magnetization is induced by the magnetic order on the Fe sublattice, leading to one common $T_N$. Different types of magnetic structures and

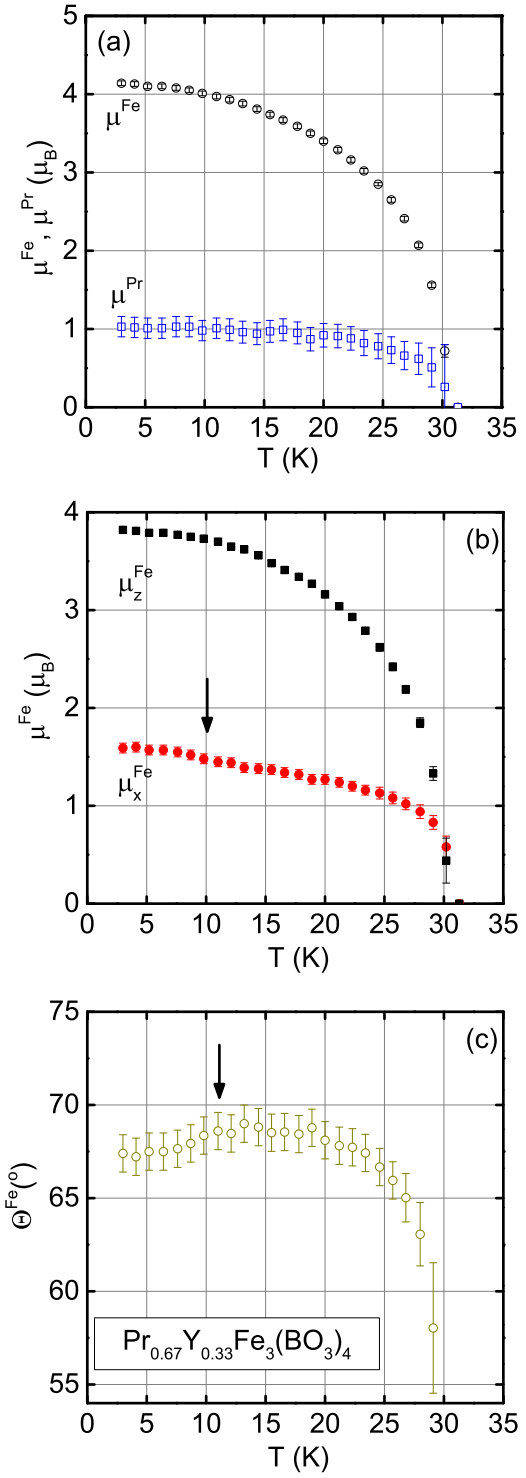


FIG. 4. (Color online) (a) Temperature dependence of the magnetic moments on the Fe and Pr sublattices. (b) The same for the individual components of the Fe moment in $z$ direction ($\mu_z^{Fe}$) and within the basal plane ($\mu_x^{Fe}$). (c) Inclination of the Fe-moment $\Theta^{Fe}$ from the basal plane as function of the temperature.

orientations of the sublattices have been related to the different strong anisotropies of the rare-earth ions. In $YFe_3(BO_3)_4$, where the rare earth is nonmagnetic, an EP magnetic structure has been found for the Fe sublattice [11] and linked to a small

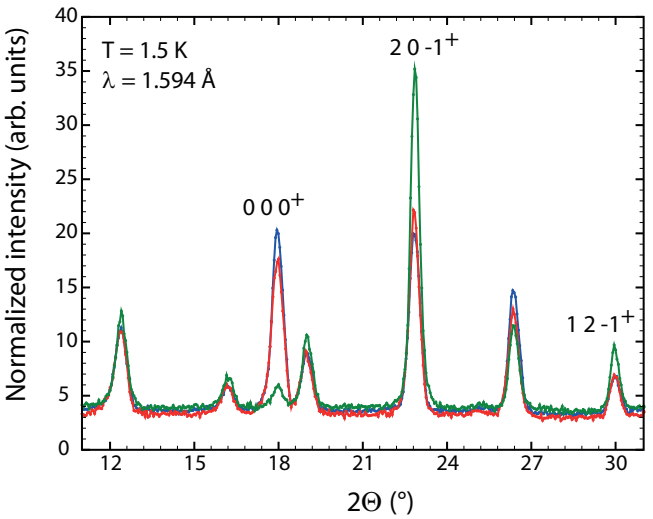


FIG. 5. (Color online) Low angle part of the neutron diffraction patterns of $Pr_{0.67}Y_{0.33}Fe_3(BO_3)_4$ (green line), $Pr_{0.55}Y_{0.45}Fe_3(BO_3)_4$ (red line), and $Pr_{0.45}Y_{0.55}Fe_3(BO_3)_4$ (blue line) measured at $T = 1.5$ K.

anisotropy of the Fe ions [12]. In the discussed compound $Pr_{0.67}Y_{0.33}Fe_3(BO_3)_4$, it is possible to follow the change of the orientation of the Fe sublattice $\Theta^{Fe}$ on approaching $T_N$: Fig. 4(c) shows that a strong decrease of $\Theta^{Fe}$ takes place between 20 K and $T_N$. This leads to a situation where the Fe sublattice approaches the basal plane orientation, as found in pure $YFe_3(BO_3)_4$, and supports the interpretation of the Fe sublattice developing first long range magnetic order which in turn induces the magnetization of the rare-earth sublattice. Trying to induce a stronger change in the spin orientation, we decided to look at compounds $Pr_xY_{1-x}Fe_3(BO_3)_4$ with $x < 0.67$ in order to reduce even further the influence of the rare-earth sublattice.

The neutron thermodiffractograms of $Pr_{0.55}Y_{0.45}Fe_3(BO_3)_4$ and $Pr_{0.45}Y_{0.55}Fe_3(BO_3)_4$ look very similar to the one of the $x = 0.67$ compound. Additional Bragg peaks of magnetic origin appearing at about 30 K can be indexed with the same magnetic propagation vector $\boldsymbol{\kappa} = [0\,0\,3/2]$. However, the relative intensity of the different magnetic peaks has significantly changed, indicating a change in the spin directions. Figure 5 displays the low angle region of the neutron patterns taken for the three compounds with $x = 0.67$, 0.55, and 0.45 at the base temperature of 1.5 K.

It can, for example, be seen in Fig. 5 that when going from $x = 0.67$ to $x = 0.45$ over $x = 0.55$, the intensity of the $(0\,0\,0)^+$ reflection increases strongly while the $(20-1)^+$ and the $(12-1)^+$ reflections are decreasing. This change of magnetic peak intensity is caused by a change in the degree of spin canting: with decreasing Pr content the magnetic moments get more aligned towards the basal plane. Figure 6(a) shows the refinement of high resolution data of the $x = 0.55$ compound at 1.5 K where $\mu^{Fe} = 4.5(1)\,\mu_B$ and $\mu^{Pr} = 0.4(4)\,\mu_B$. The size of the magnetic moment of Pr is now strongly reduced and falls within the error bars. For the refinement of the temperature evolution of the individual components of the Fe moment, it was therefore fixed to zero. Figure 6(b) shows

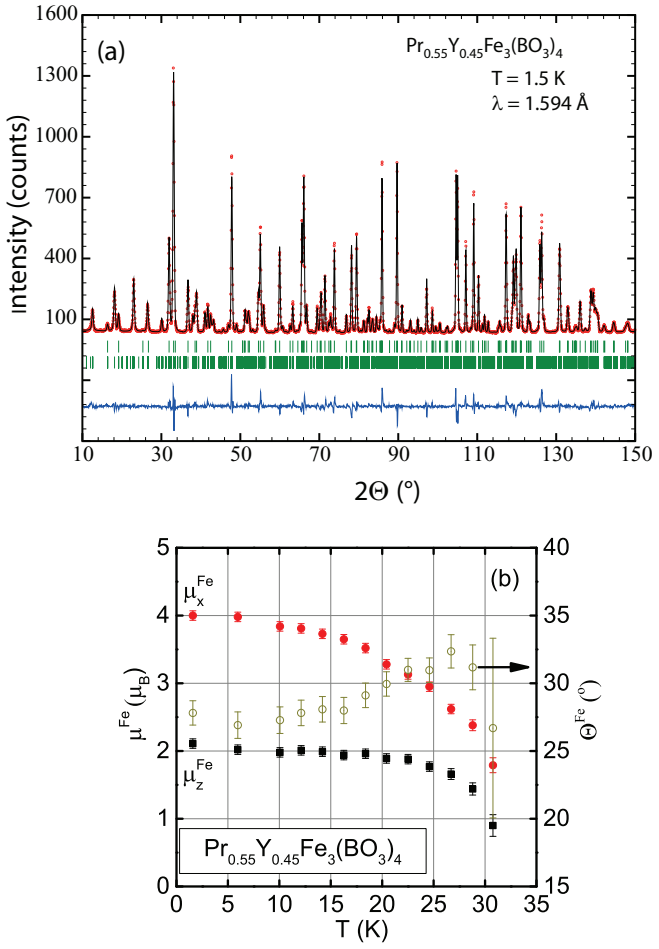


FIG. 6. (Color online) (a) Observed (red dots), calculated (black line), and difference pattern of $Pr_{0.55}Y_{0.45}Fe_3(BO_3)_4$ at 1.5 K refined in $R32$. The tick marks indicate the calculated position of the nuclear (upper row) and magnetic (lower) Bragg peaks. (b) Temperature dependence of the individual components of the Fe moment in $z$ direction ($\mu_z^{Fe}$) and within the basal plane ($\mu_x^{Fe}$) and inclination of the Fe-moment $\Theta^{Fe}$ from the basal plane as function of the temperature.

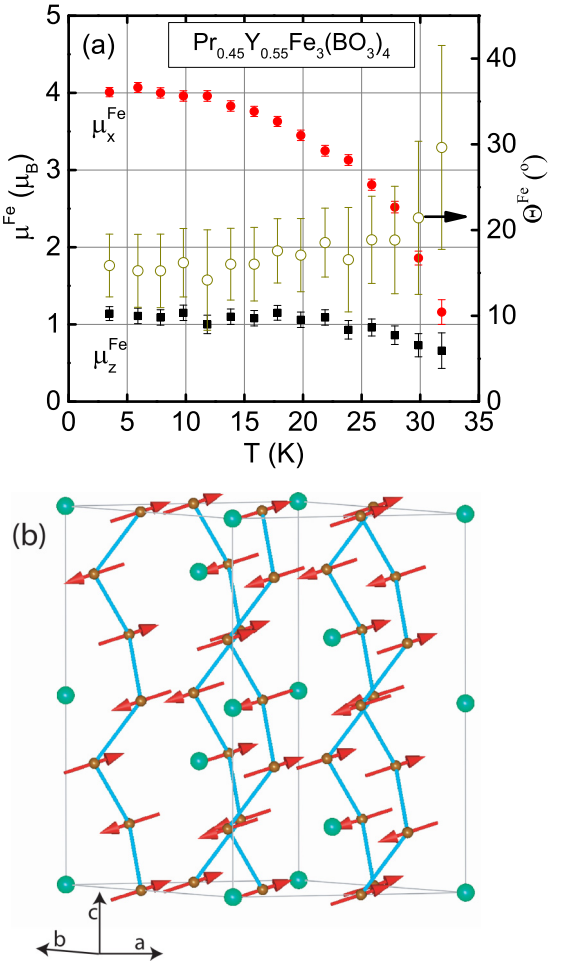


FIG. 7. (Color online) (a) Temperature dependence of the individual components of the Fe moment in $z$ direction ($\mu_z^{Fe}$) and within the basal plane ($\mu_x^{Fe}$) and inclination of the Fe-moment $\Theta^{Fe}$ from the basal plane as function of the temperature in $Pr_{0.45}Y_{0.55}Fe_3(BO_3)_4$. (b) Magnetic structure at 3 K, Fe spins in red, and the direct Fe-Fe exchange along the helicoidal chains is indicated by light blue lines.

that in $Pr_{0.55}Y_{0.45}Fe_3(BO_3)_4$, the basal plane component $\mu_x^{Fe}$ has become larger than the component in $c$ direction $\mu_z^{Fe}$. The inclination of the Fe moment from the basal plane at lowest temperature has reduced from about $\Theta^{Fe} = 67(2)^\circ$ in the $x = 0.67$ compound to the current $\Theta^{Fe} = 27(2)^\circ$. There is no sign for a spin reorientation as a function of temperature, $T_N \approx 32$ K. Neither the high resolution nor the high intensity data show any trace of the possible structural transition from $R32$ to $P3_121$.

As the Pr content gets further reduced to $x = 0.45$, it is no longer possible to detect any magnetic moment at low temperatures on the Pr site. Only the Fe sublattice seems magnetically long range ordered with $\mu^{Fe} = 4.2(1)\,\mu_B$. As expected, the magnetic structure is approaching even further than the one found for $YFe_3(BO_3)_4$. The component of the Fe moment pointing in the direction of the $c$ axis $\mu_z^{Fe}$ is further reduced, and the inclination angle decreases to about $\Theta^{Fe} = 16(4)^\circ$ at 3 K. Figure 7(a) shows that there is again no sign of a spin reorientation between $T_N \approx 33$ K and low temperature; Fig. 7(b) displays the orientation of the Fe moments. The refinement of the crystallographic structure was done in $R32$ in the whole temperature range as none of the superlattice peaks typical for the transition from $R32$ to $P3_121$ was detected.

Resuming the changes of the magnetic structure within the series of compounds $Pr_xY_{1-x}Fe_3(BO_3)_4$, one can state that unlike compounds with $R$ = Ho, Gd, and Nd-Dy systems and contrary to what had been expected, it is not possible to find a concentration $x$ for which a spontaneous temperature induced spin reorientation could be found. Instead a continuous change from the EA type magnetic structure, as found in $PrFe_3(BO_3)_4$, to the EP type magnetic structure of $YFe_3(BO_3)_4$ is seen as the value of $x$ is decreased. Figure 8 shows how the inclination of the magnetic moments on the Fe sublattice with respect to the hexagonal basal plane changes from 90° for $x = 1$ to 0° for $x = 0$ over intermediate values as function of $x$. The value of the magnetic moment on the Fe site for the doped compounds stays nearly constant with $\mu^{Fe} \approx 4.2$–$4.5\,\mu_B$ and similar to the moment value found in the pure $PrFe_3(BO_3)_4$ where $\mu^{Fe} =$

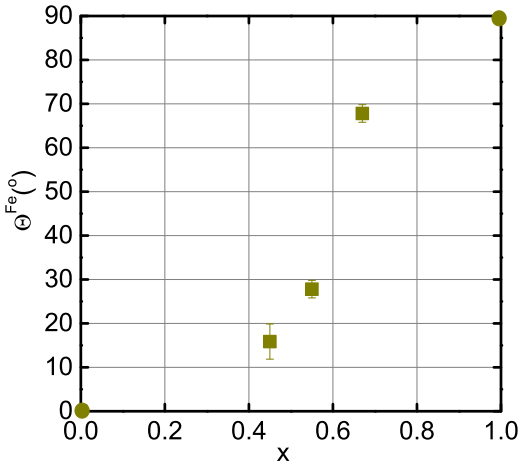


FIG. 8. (Color online) Inclination of the Fe-sublattice magnetic moment direction relative to the hexagonal basal plane as function of $x$ in $Pr_xY_{1-x}Fe(BO_3)_4$.

4.3 $\mu_B$ or to $YFe_3(BO_3)_4$ with $\mu^{Fe} = 4.0\,\mu_B$. The value of the magnetic moment per Pr ion changes from $\mu^{Pr} = 0.8(1)\,\mu_B$ in $x = 1$ over $\mu^{Pr} = 0.8(3)\,\mu_B$ for $x = 0.67$ to $\mu^{Pr} = 0.4(4)\,\mu_B$ for $x = 0.55$ before it gets too small to be detectable by neutron diffraction in the $x = 0.45$ compound. Noteworthy is the fact that in this last compound, the influence of the strongly diluted Pr sublattice is nevertheless still visible through the nonplanar component $\mu_z^{Fe}$. The magnetic transition temperature stays for $1.0 \leqslant x \leqslant 0.45$, constant at $T_N \approx 32$–33 K, noticeably below $T_N = 37$ K found for $x = 0$. If the transition temperature would follow exactly the dependence on the rare-earth ionic radius, as described by Hinatsu *et al.* [6], one would have expected $T_N$ to increase to about 35 K in $Pr_{0.45}Y_{0.55}Fe_3(BO_3)_4$.

## IV. THEORY

The magnetic properties of $Pr_xY_{1-x}Fe_3(BO_3)_4$ crystals are determined both by the magnetic subsystems and by the interaction between them. The Fe subsystem in this compound can be considered as consisting of two antiferromagnetic sublattices. The $R$ subsystem (magnetized due to the $f$-$d$ interaction) can also be represented as a superposition of two sublattices. In the calculations, we used a theoretical approach, which has been applied for description of the magnetic properties of the $RFe_3(BO_3)_4$ (see, e.g., Refs. [3,14–16,25], and [26]). This approach is based on a crystal-field model for the $R$ ion and on the molecular-field approximation. Effective Hamiltonians describing the interaction of each $R$/Fe ion in the $i$th ($i = 1, 2$) sublattice of the corresponding subsystem in the applied magnetic field $\mathbf{H}$ can be written as

$$\mathcal{H}_i(\mathrm{Pr}) = \mathcal{H}_i^{CF} - g_J\mu_B\mathbf{J}_i\left[\mathbf{H} + \lambda_{fd}\mathbf{M}_i^{Fe}\right], \tag{1}$$

$$\mathcal{H}_i(\mathrm{Fe}) = -g_S\mu_B\mathbf{S}_i\left[\mathbf{H} + \lambda\mathbf{M}_j^{Fe} + x\lambda_{fd}\mathbf{m}_i^{Pr}\right], \quad j = 1, 2, \quad j \neq i, \tag{2}$$

where $\mathcal{H}_i^{CF}$ is the crystal-field Hamiltonian, $g_J$ is the Lande factor, $\mathbf{J}_i$ is the operator of the angular moment of the $R$ ion, $g_S = 2$ is the $g$ value, $\mathbf{S}_i$ is the operator of the spin moment of an iron ion, and $\lambda_{fd} < 0$ and $\lambda < 0$ (including intrachain $\lambda_1 < 0$ and interchain $\lambda_2 < 0$) are the molecular constants of the antiferromagnetic interactions $R$–Fe and Fe–Fe, respectively. Note that the molecular constant $\lambda_{fd}$ describes the isotropic $f$-$d$ exchange interaction only. The magnetic moments of the $i$th iron $\mathbf{M}_i^{Fe}$ and rare-earth $\mathbf{m}_i^{Pr}$ sublattices per formula unit (f.u.) are defined as

$$\mathbf{M}_i^{Fe} = 3g_S\mu_B\langle\mathbf{S}_i\rangle, \quad \mathbf{m}_i^{Pr} = g_J\mu_B\langle\mathbf{J}_i\rangle. \tag{3}$$

The crystal-field Hamiltonian $\mathcal{H}^{CF}$ can be expressed using irreducible tensor operators $C_q^k$ as

$$\mathcal{H}^{CF} = B_0^2C_0^{(2)} + B_0^4C_0^{(4)} + iB_{-3}^4\left(C_{-3}^{(4)} + C_3^{(4)}\right) + B_0^6C_0^{(6)} + iB_{-3}^6\left(C_{-3}^{(6)} + C_3^{(6)}\right) + B_6^6\left(C_{-6}^{(6)} + C_6^{(6)}\right), \tag{4}$$

For the $Pr^{3+}$ ion in $Pr_xY_{1-x}Fe_3(BO_3)_4$ ($x = 0.67, 0.55, 0.45$), the crystal-field parameters $B_q^k$ are unknown, and data on the splitting of the ground-state multiplet are unavailable. Therefore, to calculate the magnetic characteristics of $Pr_xY_{1-x}Fe_3(BO_3)_4$, we used the parameters of the crystal field for pure $PrFe_3(BO_3)_4$ from Ref. [20].

In order to calculate the magnitudes and orientations of the magnetic moments in the Fe and $R$ subsystems, it is necessary to solve a self-consistent problem based on Hamiltonians (1, 2) under the condition of minimum for the corresponding thermodynamic potential (see, e.g., Refs. [15,16], and [26]). Then, it is possible to determine the regions of stability of various magnetic phases, the critical fields for the phase transitions, the magnetization curves, the magnetic susceptibilities, etc.

The anisotropy energy for the $i$th sublattice of the Fe subsystem for a crystal of trigonal symmetry can be written as

$$\Phi_{an}^i = K_2^{Fe}\sin^2\vartheta_i + K_4^{Fe}\sin^4\vartheta_i + K_{66}^{Fe}\sin^6\vartheta_i\cos 6\varphi_i, \tag{5}$$

where an anisotropy constant $K_2^{Fe} < 0$ stabilizes the EP state; a constant $K_4^{Fe} > 0$ stabilizes the EA state; $K_{66}^{Fe} < 0$ is the anisotropy constant in the basal $ab$ plane ($K_{66}^{Fe} = -0.135$ kOe · $\mu_B$ [15,16]); and $\vartheta_i$ and $\varphi_i$ are the polar and azimuth angles of magnetic moment $\mathbf{M}_i^{Fe}$ of iron, respectively.

The magnetization and magnetic susceptibility of the compound (per f.u.) are defined as

$$\mathbf{M} = \frac{1}{2}\sum_{i=1}^{2}\left(\mathbf{M}_i^{Fe} + x\mathbf{m}_i^{Pr}\right), \quad \chi_k = \chi_k^{Fe} + x\chi_k^{Pr}, \quad k = a, b, c. \tag{6}$$

## V. COMPARISON OF EXPERIMENTAL DATA AND THEORETICAL CALCULATIONS

To describe the neutron data, one should first define the parameters of the exchange interactions and anisotropy constants, which can be obtained by fitting to the experimental field and temperature dependences of the magnetization for selected samples. Fragments of the magnetic data that are used to find relevant parameters are given below. The complete experimental data on magnetic and resonance measurements for the entire family of crystals will be given in a separate paper.

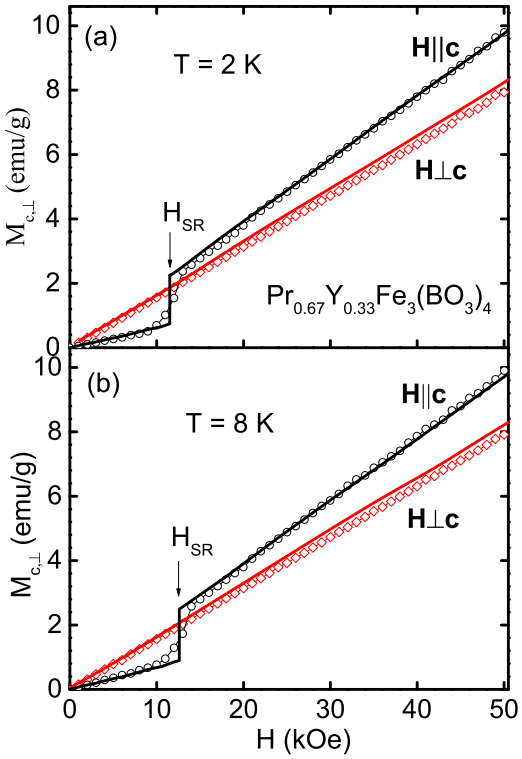


FIG. 9. (Color online) Experimental (symbols) and calculated (lines) magnetization curves of $Pr_{0.67}Y_{0.33}Fe_3(BO_3)_4$ for $\mathbf{H}\|\mathbf{c}$ and $\mathbf{H}\perp\mathbf{c}$ at $T = 2$ K (a) and $T = 8$ K (b).

The field dependences of the magnetization $M_c(H)$ and $M_\perp(H)$ measured for the sample $Pr_{0.67}Y_{0.33}Fe_3(BO_3)_4$ at 2 and 8 K are shown in Figs. 9(a) and 9(b). In this sample, as follows from the neutron data, the orientation of the magnetic moments of the iron ions is still close to the $c$ axis (the inclination from the basal plane is $\Theta^{Fe} = 67^\circ$), so the spin-floplike spin reorientation occurs at $H_{SR} \approx 11.5$ kOe for $T = 2$ K and at $H_{SR} \approx 12.5$ kOe for $T = 8$ K when the magnetic field is directed along the $c$ axis. A similar reorientation is faintly discernible in the data for the crystal with $x = 0.55$, which has an intermediate value of $\Theta^{Fe} = 27^\circ$. In the crystal with $x = 0.45$, the neutron data showed that the iron moments are almost in the basal plane with $\Theta^{Fe} = 16^\circ$, and accordingly a linear behavior of $M_c(H)$ with no signs of a spin-reorientation is found for $x = 0.45$. Thus, the changes in the field dependences of the magnetization confirm the fact that the magnetic moments of iron tilt closer to the basal plane as the content of praseodymium is reduced.

The theoretical dependences presented in Figs. 9–12 were calculated using parameters given in Table III. The values of these parameters were chosen from the requirement of the best agreement between the calculated and experimental curves at all temperatures. All the experimental data are considered simultaneously, and a sensitivity of the individual experimental dependences to the given parameters is analyzed.

The parameters $\lambda_1$ and $\lambda_2$, which define the exchange fields $H_{dd1} = \lambda_1 M_0^{Fe}$ and $H_{dd2} = \lambda_2 M_0^{Fe}$, were chosen from the best agreement between experimental and calculated magnetization curves $M_{c,\perp}(H)$ at $T = 2$, 8, 20, and 30 K. For the high-field region $H > H_{SR}$, the slope of the magnetization

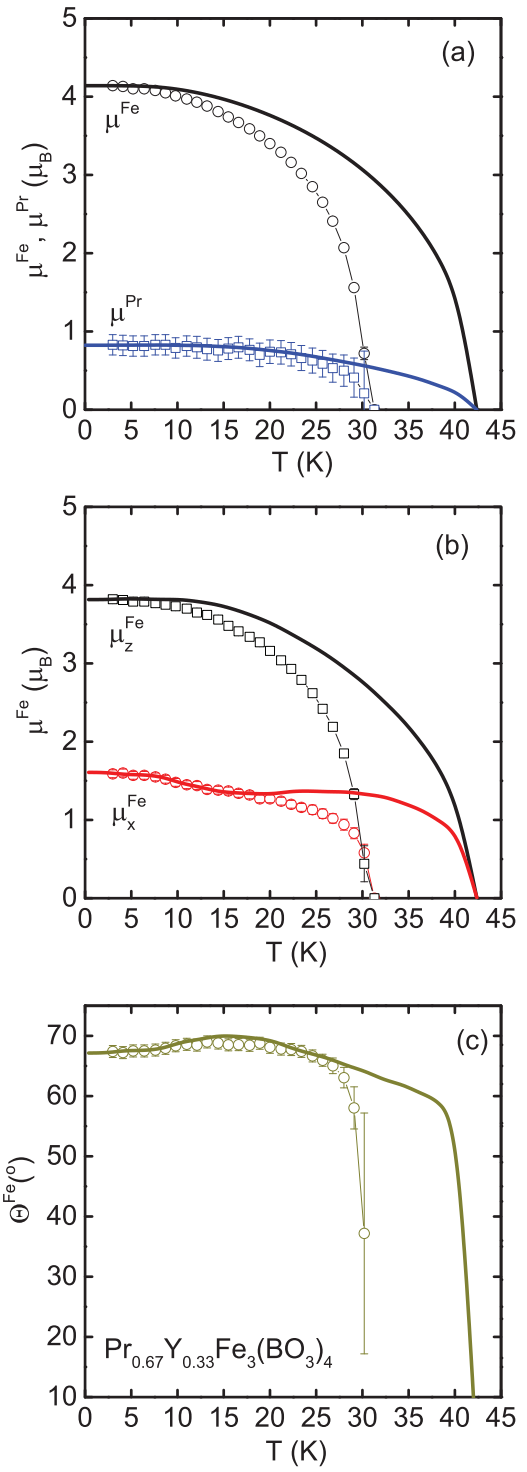


FIG. 10. (Color online) (a) Experimental (symbols) and calculated (lines) temperature dependence of the magnetic moments of the Fe and Pr sublattices of $Pr_{0.67}Y_{0.33}Fe_3(BO_3)_4$. (b) The same for the individual components of the Fe moment in $z$ direction ($\mu_z^{Fe}$) and within the basal plane ($\mu_x^{Fe}$). (c) Inclination of the Fe moment from the basal plane as a function of the temperature.

curve is determined by the parameter $\lambda_1$ of the intrachain Fe-Fe exchange interaction, since it is mainly this interaction that prevents the rotation of the magnetic moments of the iron subsystem in the flop phase toward the field direction. The

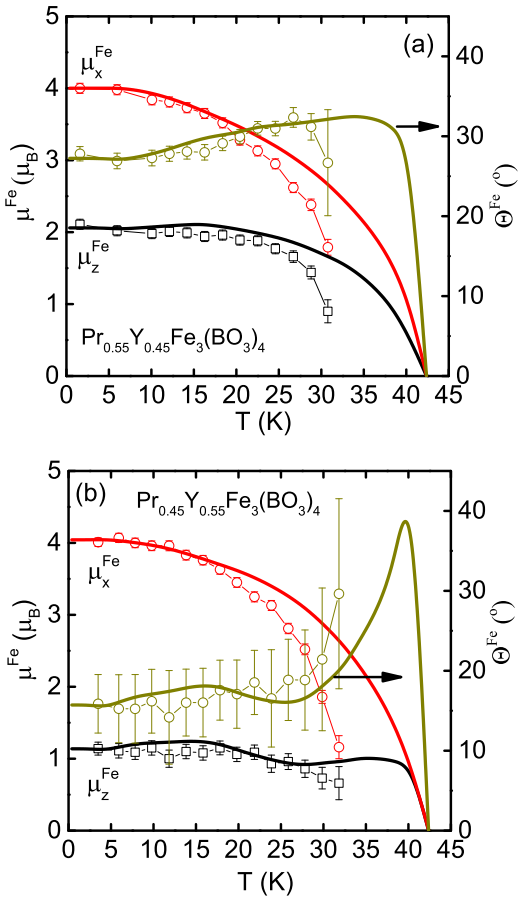


FIG. 11. (Color online) Experimental (symbols) and calculated (lines) temperature dependence of the individual components of the Fe moment in $z$ direction ($\mu_z^{Fe}$) and within the basal plane ($\mu_x^{Fe}$) and inclination of the Fe moment from the basal plane as functions of the temperature for $Pr_{0.55}Y_{0.45}Fe_3(BO_3)_4$ (a) and $Pr_{0.45}Y_{0.55}Fe_3(BO_3)_4$ (b).

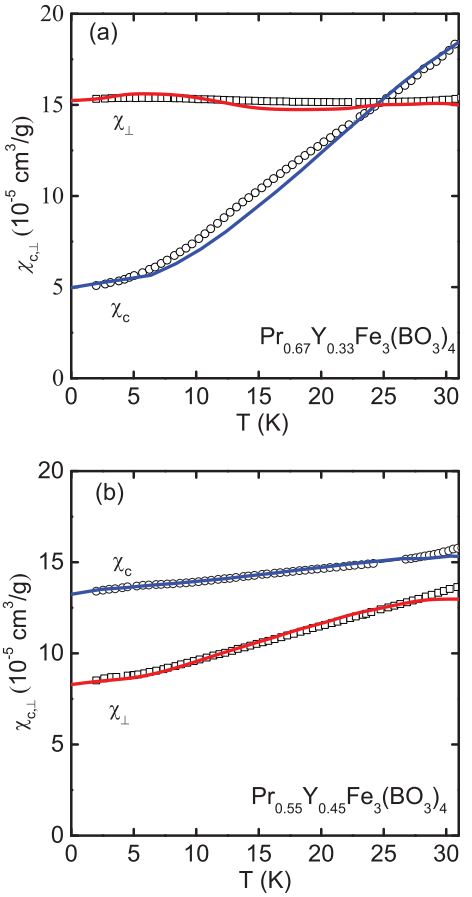


FIG. 12. (Color online) Experimental (symbols) and calculated (lines) temperature dependencies of the initial magnetic susceptibility $\chi_{c,\perp}(T)$ of $Pr_{0.67}Y_{0.33}Fe_3(BO_3)_4$ (a) and $Pr_{0.55}Y_{0.45}Fe_3(BO_3)_4$ (b) at $H = 1$ kOe.

parameter $\lambda_2$ appearing in the Brillouin function is mainly responsible for the value of the magnetic moment of iron at a given temperature, and a given magnetic field and determines the Néel temperature. It was chosen from the best agreement between experimental and calculated magnetization curves for all temperatures.

As can be seen from Fig. 9, the calculation using parameters of the crystal field for pure $PrFe_3(BO_3)_4$ [20] and chosen parameters $\lambda_1$ and $\lambda_2$ describes well the slope of the experimental curves $M_{c,\perp}(H)$ in $Pr_{0.67}Y_{0.33}Fe_3(BO_3)_4$ at $H > H_{SR}$. A similar description of the high-field parts of the experimental curves $M_{c,\perp}(H)$ has been achieved for the compositions with $x = 0.55$ and 0.45. Note that the values of $H_{dd1}$ and $H_{dd2}$ found here for $Pr_xY_{1-x}Fe_3(BO_3)_4$ (see Table III) are little different from those for pure $PrFe_3(BO_3)_4$ given in [14] where $H_{dd1} = 430$ kOe and $H_{dd2} = 250$ kOe.

At low temperature and fixed parameters of the crystal field, the magnetic moment of the $Pr_x$ subsystem $\mu_{calc}^{Pr}$ can be modified only by the change of the parameter $\lambda_{fd}$ defining the $f$-$d$ exchange field $H_{fd} = \lambda_{fd}M_0$. For each of the compounds, we defined the parameter $\lambda_{fd}$ so as to reproduce the experimental value of $\mu_{exp}^{Pr}$. As a result, the calculation of the $M_{c,\perp}(H)$ curves with parameters of the crystal field from Ref. [20], and chosen parameters ($\lambda_1$, $\lambda_2$ and $\lambda_{fd}$) provides throughout the entire field range a good description of the behavior of the corresponding experimental curves in Fig. 9.

Constants $K_2^{Fe}$ and $K_4^{Fe}$ were determined for each of the compounds from the condition of the best description of the low-temperature value of the angle inclination of the Fe moment from the basal plane $\Theta_{exp}^{Fe}$ at $T = 3$ K. Then, with the chosen parameters ($\lambda_1$, $\lambda_2$, and $\lambda_{fd}$), we fitted the temperature dependences of the constants $K_2^{Fe}$ and $K_4^{Fe}$, which decrease with temperature, and reproduce the main features of the experimental dependencies $\Theta_{exp}^{Fe}(T)$. Note that the obtained large values of the constants $K_2^{Fe}$ stabilizing the EP alignment of the magnetic subsystem are apparently caused by using the crystal-field parameters of the pure EA compound $PrFe_3(BO_3)_4$ [20] in the calculation. Only the experimental study of spectroscopic, magnetic (in a wide range of magnetic fields and temperatures) and thermal (heat capacity) properties of $Pr_xY_{1-x}Fe_3(BO_3)_4$ ($x = 0.67, 0.55, 0.45$) will allow to determine the crystal-field parameters for $Pr^{3+}$ in diamagnetically diluted compounds and provide the corrected values of the magnetic anisotropy constants for the iron subsystem.

Table III shows that a significant reduction of $\mu^{Pr}$, both calculated and measured, takes place as parameter $x$ decreases

TABLE III. Parameters of $Pr_xY_{1-x}Fe_3(BO_3)_4$ : the intrachain Fe-Fe exchange field $H_{dd1}$, the interchain Fe-Fe exchange field $H_{dd2}$, and the $f$-$d$ exchange field $H_{fd}$ are the low temperature exchange fields corresponding to the molecular constants $\lambda_1$, $\lambda_2$, and $\lambda_{fd}$, respectively; $M_0^{Fe}$ is the magnetic moment of iron per f.u.; $\mu_{calc}^{Pr}/\mu_{exp}^{Pr}$ are calculated/experimental magnetic moments of praseodymium ($\mu_{calc}^{Pr} = xm^{Pr}$); $K_2^{Fe}$ and $K_4^{Fe}$ are the uniaxial anisotropy constants.

| | $x = 0.67$ | $x = 0.55$ | $x = 0.45$ |
|---|---|---|---|
| $H_{dd1} = \lambda_1 M_0^{Fe}$, kOe | 351 | 351 | 351 |
| $H_{dd2} = \lambda_2 M_0^{Fe}$, kOe | 263 | 263 | 264 |
| $H_{fd} = \lambda_{fd} M_0^{Fe}$, kOe | 178.5 | 178 | 170 |
| $M_0^{Fe} = \lvert M_i^{Fe}(T = 0, H = 0)\rvert$, $\mu_B$ | 3·4.2 | 3·4.5 | 3·4.2 |
| $\mu_{calc}^{Pr}/\mu_{exp}^{Pr}$ ($T = 3$ K), $\mu_B$ | 0.82/0.8(3) | 0.40/0.4(4) | 0.22/– |
| $K_2^{Fe}$ ($T = 3$ K), kOe · $\mu_B$ | –93.2 | –93 | –90 |
| $K_4^{Fe}$ ($T = 3$ K), kOe · $\mu_B$ | 9.94 | 9.9 | 10 |

from 0.67 to 0.55. This has to be related to the fact that the magnetic moment $\mu^{Pr}$ in the EA, inclined, and EP states depends on the splitting of the lowest energy levels of the ion. Due to the $f$-$d$ exchange interaction, the Pr subsystem adds the EA contribution to the total magnetic anisotropy of the crystal. As the diamagnetic dilution increases with decreasing $x$, the magnetic moments of the iron ions tilt progressively towards the basal plane. At the same time the magnetic moments of the ions $Pr^{3+}$, which are connected with the iron moments by the $f$-$d$ interaction, tilt more to the basal plane reducing thereby the splitting of the lowest energy levels of $Pr^{3+}$ leading to a reduction of the magnetic moment $\mu^{Pr}$.

The agreement between calculations and experimental data for $Pr_{0.67}Y_{0.33}Fe_3(BO_3)_4$ is quite good at low temperatures (see Fig. 10); however, it becomes less satisfactory on approaching the Néel temperature. For all the compounds, the calculated Néel temperatures are higher than the corresponding experimental values, a disagreement often found when using mean-field theory [34].

Taking into account that $\mu_{exp}^{Pr}$ obtained from the high intensity D1B data seems overstated in comparison with the more accurate D2B data as explained in Ref. [33], the calculated temperature dependence $\mu_{exp}^{Pr}(T)$ in Fig. 10(a) is compared with the experimental one from Fig. 4(a), normalized to the value of 0.8 $\mu_B$ at low temperatures. Note that the calculated curves reflect all the main features of the experimental curves, for example, the nonmonotonic behavior of the curve $\Theta_{exp}^{Fe}(T)$ in the range of 5–20 K [Fig. 10(c)] and a faintly discernible inflection of the curve $\mu_x^{Fe}(T)$ [Fig. 10(b)]. Similar results describing the experimental data for the compositions with $x = 0.55$ and 0.45 are presented in Fig. 11.

Figure 12 shows the low-temperature regions (at $T < T_N$) of the experimental and calculated dependences of the magnetic susceptibilities $\chi_{c,\perp}(T)$ of $Pr_{0.67}Y_{0.33}Fe_3(BO_3)_4$ and $Pr_{0.55}Y_{0.45}Fe_3(BO_3)_4$.

As the influence of the applied field on $\Theta_{exp}^{Fe}(T)$ when measuring in magnetic fields $\mathbf{H}\|\mathbf{c}$ and $\mathbf{H}\perp\mathbf{c}$ is not known, the temperature dependence of the susceptibilities $\chi_{c,\perp}(T)$ for $x = 0.67$ and 0.55 (Fig. 12) were calculated using the anisotropy constants, and their temperature dependences as defined at $H = 0$. Some of the differences between the experimental and the calculated dependences in this figure can be connected just to the influence of the applied field.

There is a slightly pronounced maximum near 15 K in the experimental curve $\chi_c(T)$ for $Pr_{0.67}Y_{0.33}Fe_3(BO_3)_4$ [Fig. 12(a)]. Analysis shows that this cannot be related to a Schottky anomaly because the splitting between the lowest energy levels $\Delta \approx 72\,cm^{-1}$ is too large. The maximum can be explained by the nonmonotonic change in the angle of inclination $\Theta_{exp}^{Fe}(T)$. On the calculated curve $\chi_c(T)$, this maximum is shifted to a higher temperature ~27 K due to the abovementioned shortcomings of the mean-field theory.

Remember that the single set of parameters of the crystal field of the pure EA compound $PrFe_3(BO_3)_4$ was used for all three compounds with $x = 0.67, 0.55, 0.45$ for obtaining the parameters given in the Table III and the calculated curves in Figs. 9–12. It is clear that the environment of the rare-earth ion depends on $x$, so the parameters of the crystal field for different compositions should be slightly different. A detailed analysis of the magnetic properties for this family of crystals in magnetic fields up to 50 kOe is planned and will be done in the area of critical concentrations ($x = 0.67$–$0.45$) corresponding to the inclined magnetic structure, as well as for $Pr_{0.75}Y_{0.25}Fe_3(BO_3)_4$ and $Pr_{0.25}Y_{0.75}Fe_3(BO_3)_4$ with EA and EP magnetic structures, respectively. The frequency-field and the temperature dependences of magnetic resonance will be also measured and analyzed for the entire family of compounds $Pr_xY_{1-x}Fe_3(BO_3)_4$. Such an analysis will complement the results in zero magnetic field presented in this paper and will allow us to determine the individual set of crystal-field parameters for each of the compounds.

## VI. CONCLUSIONS

Single crystals of the family of $Pr_xY_{1-x}Fe_3(BO_3)_4$ of about 4–6 mm in size were grown from the flux. High resolution and temperature dependent high intensity powder neutron diffraction studies as well as magnetic measurements were carried out on $Pr_xY_{1-x}Fe_3(BO_3)_4$ with the concentration $x =$ 0.67–0.45. As in other rare-earth ferroborates $RFe_3(BO_3)_4$, the magnetic order appears simultaneously in the subsystems of $Fe^{3+}$ and $Pr^{3+}$ ions due to the $f$-$d$ exchange interaction at the Néel temperature, which stays almost constant at $T_N \approx 31$–$33$ K for $0.67 \leqslant x \leqslant 0.45$. A transition from the EA to the EP state occurs in this concentration range through the formation of inclined magnetic structures. The inclination of the Fe moments from the basal plane depends on the Pr content and ranges from 67(2)° for $x = 0.67$ to 16(4)° for $x = 0.45$ at $T = 3$ K. A nonmonotonic change of the inclination angle with temperature is found for all compounds, but there is no

sign of a spontaneous spin reorientation in the temperature range of magnetic order in none of samples studied.

The value of the magnetic moment on the Fe site stays for all the compounds nearly constant with $\mu^{Fe} \approx 4.2 - 4.5\,\mu_B$, while the magnetic moment of the Pr ion reduces strongly from $\mu^{Pr} = 0.8(3)\,\mu_B$ for $x = 0.67$ to $\mu^{Pr} = 0.4(4)\,\mu_B$ for $x = 0.55$ and becomes too small to be detectable by neutron diffraction in the $x = 0.45$ compound.

A theoretical approach based on a crystal-field model for the $Pr^{3+}$ ion and on the molecular-field approximation allows us to describe the magnetic characteristics of $Pr_xY_{1-x}Fe_3(BO_3)_4$, giving a good agreement between the experimental and calculated dependencies of $\mu^{Fe}(T)$, $\mu^{Pr}(T)$, $\Theta^{Fe}(T)$ and of the temperature dependences of the initial magnetic susceptibility $\chi_{c,\perp}(T)$.

## ACKNOWLEDGMENTS

This paper was supported by the Russian Foundation for Basic Research (Project No. 13-02-12442 ofi_m2).

[1] A. K. Zvezdin, S. S. Krotov, A. M. Kadomtseva, G. P. Vorob'ev, Y. F. Popov, A. P. Pyatakov, L. N. Bezmaternykh, and E. A. Popova, JETP Lett. **81**, 272 (2005).

[2] A. K. Zvezdin, G. P. Vorob'ev, A. M. Kadomtseva, Y. F. Popov, A. P. Pyatakov, L. N. Bezmaternykh, A. V. Kuvardin, and E. A. Popova, JETP Lett. **83**, 509 (2006).

[3] E. A. Popova, D. V. Volkov, A. N. Vasiliev, A. A. Demidov, N. P. Kolmakova, I. A. Gudim, L. N. Bezmaternykh, N. Tristan, Yu. Skourski, B. Büchner, C. Hess, and R. Klingeler, Phys. Rev. B **75**, 224413 (2007).

[4] R. P. Chaudhury, F. Yen, B. Lorenz, Y. Y. Sun, L. N. Bezmaternykh, V. L. Temerov, and C. W. Chu, Phys. Rev. B **80**, 104424 (2009).

[5] A. M. Kadomtseva, Y. F. Popov, G. P. Vorob'ev, A. P. Pyatakov, S. S. Krotov, K. I. Kamilov, V. Y. Ivanov, A. A. Mukhin, A. K. Zvezdin, A. M. Kuz'menko, L. N. Bezmaternykh, I. A. Gudim, and V. L. Temerov, Low Temp. Phys. **36**, 511 (2010).

[6] Y. Hinatsu, Y. Doi, K. Ito, M. Wakeshima, and A. Alemi, J. Solid State Chem. **172**, 438 (2003).

[7] S. A. Klimin, D. Fausti, A. Meetsma, L. N. Bezmaternykh, P. H. M. van Loosdrecht, and T. T. M. Palstra, Acta Crystallogr. B **61**, 481 (2005).

[8] C. Ritter, A. Vorotynov, A. Pankrats, G. Petrakovskiĭ, V. Temerov, I. Gudim, and R. Szymczak, J. Phys.: Condens. Matter **22**, 206002 (2010). Table I of this reference contains several errors: The right hand side (marked "Er"), not the left hand side, of the table corresponds to $PrFe_3(BO_3)_4$; values of the lattice parameters given are wrong and correspond to the Ho-compound. Atomic coordinates and interatomic distances are correct.

[9] C. Ritter, A. Pankrats, I. Gudim, and A. Vorotynov, J. Phys.: Condens. Matter **24**, 386002 (2012).

[10] E. A. Popova, A. N. Vasiliev, V. L. Temerov, L. N. Bezmaternykh, N. Tristan, R. Klingeler, and B. Buchner, J. Phys.: Condens. Matter **22**, 116006 (2010).

[11] C. Ritter, A. Vorotynov, A. Pankrats, G. Petrakovskiĭ, V. Temerov, I. Gudim, and R. Szymczak, J. Phys.: Condens. Matter **20**, 365209 (2008).

[12] A. I. Pankrats, G. A. Petrakovskiĭ, L. N. Bezmaternykh, and V. L. Temerov, Phys. Solid State **50**, 79 (2008).

[13] C. Lee, J. Kang, K. H. Lee, and M.-H. Whangbo, Chem. Mater. **21**, 2534 (2009).

[14] A. A. Demidov, N. P. Kolmakova, D. V. Volkov, and A. N. Vasiliev, Physica B **404**, 213 (2009).

[15] A. A. Demidov, I. A. Gudim, and E. V. Eremin, JETP **115**, 815 (2012).

[16] A. I. Begunov, A. A. Demidov, I. A. Gudim, and E. V. Eremin, JETP **117**, 862 (2013).

[17] D. Neogy, K. N. Chattopadhay, P. K. Chakrabarti, H. Sen, and B. M. Wanklyn, J. Phys. Chem. Solids **59**, 783 (1997).

[18] P. Fischer, V. Pomjakushin, D. Sheptyakov, L. Keller, M. Janoschek, B. Roessli, J. Schefer, G. Petrakovskiĭ, L. Bezmaternykh, V. Temerov, and D. Velikanov, J. Phys.: Condens. Matter **18**, 7975 (2006).

[19] C. Ritter, A. Balaev, A. Vorotynov, G. Petrakovskiĭ, D. Velikanov, V. Temerov, and I. Gudim, J. Phys.: Condens. Matter **19**, 196227 (2007).

[20] M. N. Popova, T. N. Stanislavchuk, B. Z. Malkin, and L. N. Bezmaternykh, Phys. Rev. B **80**, 195101 (2009).

[21] M. Janoschek, P. Fischer, J. Schefer, B. Roessli, V. Pomjakushin, M. Meven, V. Petricek, G. Petrakovskiĭ, and L. Bezmaternikh, Phys. Rev. B **81**, 094429 (2010).

[22] H. Mo, C. S. Nelson, L. N. Bezmaternykh, and V. T. Temerov, Phys. Rev. B **78**, 214407 (2008).

[23] A. I. Pankrats, G. A. Petrakovskiĭ, L. N. Bezmaternykh, and O. A. Bayukov, JETP **99**, 766 (2004).

[24] A. Pankrats, G. Petrakovskiĭ, A. Kartashev, E. Eremin, and V. Temerov, J. Phys.: Condens. Matter **21**, 436001 (2009).

[25] A. A. Demidov, I. A. Gudim, and E. V. Eremin, Physica B **407**, 393 (2012).

[26] A. A. Demidov, I. A. Gudim, and E. V. Eremin, JETP **114**, 259 (2012).

[27] A. I. Pankrats, G. A. Petrakovskiĭ, V. I. Tugarinov, A. V. Kartashev, and V. L. Temerov, JETP **113**, 483 (2011).

[28] A. M. Kadomtseva, Yu. F. Popov, G. P. Vorob'ev, A. A. Mukhin, V. Yu. Ivanov, A. M. Kuz'menko, and L. N. Bezmaternykh, JETP Lett. **87**, 39 (2008).

[29] L. N. Bezmaternykh, V. L. Temerov, I. A. Gudim, and N. A. Stolbovaya, Crystallogr. Rep. **50**, S97 (2005).

[30] J. Rodriguez-Carvajal, Physica B **192**, 55 (1993).

[31] J. Rodriguez-Carvajal, BASIREPS: a program for calculating irreducible representations of space groups and basis functions for axial and polar vector properties. Part of the FullProf Suite of programs, www.ill.eu/sites/fullprof/.

[32] C. Ritter, Solid State Phenom. **170**, 263 (2011).

[33] Atom coordinates and thermal B factors were kept fixed to the values determined from the high resolution D2B refinement of the 1.5 K data. Probably due to the more limited Q range of the high intensity D1B data, the total refined magnetic moment of the rare-earth site is slightly larger than that from D2B.

[34] J. S. Smart, *Effective Field Theories of Magnetism* (W. B. Saunders Company, Philadelphia-London, 1966).